Catal Lett (2008) 122:176–182
DOI 10.1007/s10562-007-9366-4

Gas Phase Hydrogenation of Maleic Anhydride to γ-Butyrolactone by Cu–Zn–Ce Catalyst in the Presence of *n*-Butanol

Dongzhi Zhang · Hengbo Yin · Ruichao Zhang · Jinjuan Xue · Tingshun Jiang

Received: 29 September 2007 / Accepted: 17 November 2007 / Published online: 11 December 2007

Abstract A series of Cu–Zn–Ce catalysts were prepared by coprecipitation method and characterized by X-ray diffraction, X-ray photoelectron spectroscopy, temperature programmed reduction, and N_2 adsorption. The catalytic activities of the Cu–Zn–Ce catalysts in gas phase hydrogenation of maleic anhydride in the presence of *n*-butanol were studied at 220–280 °C and 1 MPa. The conversion of maleic anhydride was more than 97%. After reduction, CuO species present in the calcined Cu–Zn–Ce catalysts were converted to metallic copper (Cu°). The presence of ZnO in the Cu–Zn–Ce catalysts was beneficial to stabilizing the catalytic activity in maleic anhydride hydrogenation to γ-butyrolactone. At the same time, *n*-butanol was dehydrogenated to butyl aldehyde, then to butyl butyrate via reactions, such as disproportionation and esterification. Cu–Zn–Ce catalysts are beneficial to the H_2 compensation in the coupling process of hydrogenation and dehydrogenation.

Keywords Maleic anhydride · Hydrogenation · γ-Butyrolactone · Cu–Zn–Ce catalysts

1 Introduction

Hydrogenation of maleic anhydride (MA) has recently attracted a great deal of attention since the hydrogenated products, such as γ-butyrolactone (GBL) and tetrahydrofuran (THF), are very important industrial chemicals. GBL is an alternative to the environmentally harmful chlorinated solvent and also an intermediate widely used in the polymer industry [1, 2].

γ-Butyrolactone is mainly produced by two processes: Reppe process based on acetylene–formaldehyde condensation and Davy McKee process based on hydrogenation of diethyl or dimethyl maleate [3]. Compared with the above-mentioned processes, direct hydrogenation of MA to GBL is the most economic way without using hazardous or carcinogenic feedstock. Furthermore, MA has been produced in a large scale by partial oxidation of *n*-butane, a by-product from petroleum industry, over the last decades, which is another advantage in MA hydrogenation to GBL [4].

Noble and transition metals are commonly used as the active components of the hydrogenation catalysts. For the catalytic hydrogenation of MA, Hara and Takahashib [1] investigated the liquid phase hydrogenation of MA to GBL catalyzed by a series of Ru complexes with exceeding 97% selectivity of GBL. Jung et al. [2] reported that Pd–Sn/SiO_2 can be used as an effective one-step catalyst for hydrogenation of MA to GBL. Although the noble metals, such as Ru and Pd, show excellent performance in the direct hydrogenation of MA to GBL, the production cost would be quite high if noble metals were used as the catalysts.

Copper-based catalysts have been widely investigated in the MA hydrogenation process in liquid phase at pressures between 5 and 9 MPa and temperatures between 200 and 240 °C [5, 6], and in gas phase at atmospheric pressure and temperatures between 210 and 280 °C [4, 7, 8]. Cu/ZnO/M_xO (M = Al, Cr, Ti, etc.) catalysts are commonly used in the gas phase hydrogenation of MA. In the above-mentioned catalysts, zinc and chromium oxides are usually used as the dispersant and support of the active metal component. The presence of titania promotes the activity of Cu/ZnO catalyst in MA hydrogenation to GBL [4]. Recently, cerium oxide has been found as a functional

D. Zhang · H. Yin (✉) · R. Zhang · J. Xue · T. Jiang
Faculty of Chemistry and Chemical Engineering,
Jiangsu University, Zhenjiang 212013, P.R. China
e-mail: yin@ujs.edu.cn

component of catalysts for oxidation and reduction reactions since cerium oxide has redox property [9, 10]. Since MA hydrogenation is a reduction process, it can be predicted that CeO_2 as an alternative to Cr or Al present in copper-based catalyst should have a positive impact on the selective hydrogenation of MA.

Recently, coupling of an exothermic hydrogenation reaction and an endothermic dehydrogenation reaction in one reaction system attracted researchers' interest in view of thermodynamics [11–13]. Copper-based catalysts not only catalyze the exothermic gas phase hydrogenation of MA but also catalyze the endothermic gas phase dehydrogenation of linear primary alcohols with *n* carbon atoms to corresponding valuable aldehyde and ester with 2*n* carbon atoms instead of the traditional esterification catalyst H_2SO_4 [14, 15]. In the hydrogenation process of MA, producing 1 mol GBL requires 1 mol MA and 3 mol H_2; producing 1 mol THF requires 1 mol MA and 5 mol H_2; producing 1 mol dibutyl succinate requires 1 mol MA and 1 mol H_2 [4, 16, 17]. In the dehydrogenation process of *n*-butanol catalyzed by copper-based catalysts, *n*-butanol is dehydrogenated to butyl aldehyde and butyl butyrate. Producing 1 mol butyl aldehyde requires 1 mol *n*-butanol, releasing 1 mol H_2; producing 1 mol butyl butyrate requires 2 mol *n*-butanol, releasing 2 mol H_2 [4, 14, 15]. It can be predicated that the coupling of hydrogenation of MA and dehydrogenation of a linear primary alcohol, such as *n*-butanol, in one reaction system using a copper-based catalyst should be beneficial to the two reactions in view of the compensation of H_2.

In this paper, we reported a study on the hydrogenation of MA in the presence of *n*-butanol over Cu–Zn–Ce catalysts prepared by coprecipitation method at 220–280 °C and 1 MPa. The major objective of this work is to gain an insight into the catalytic activity of Cu–Zn–Ce catalysts in the hydrogenation of MA to GBL and the dehydrogenation of *n*-butanol to butyl aldehyde and butyl butyrate.

2 Experimental

2.1 Catalyst Preparation

The Cu–Zn–Ce catalysts were prepared by a continuous coprecipitation method. A mixed solution of $Cu(NO_3)_2 \cdot 3H_2O$, $Zn(NO_3)_2 \cdot 6H_2O$, and $Ce(NO_3)_2 \cdot 6H_2O$ salts with a given atomic ratio was used as a precursor solution, and 1 M Na_2CO_3 solution was used as the precipitating agent. Coprecipitation was performed at 75 °C in a supersonic reactor. The flow rates of the two solutions were adjusted to give a constant pH value of ca. 8. The resultant suspension was aged for 12 h at room temperature. The precipitate was filtrated and washed with distilled water until the conductivity of the filtrate was less than 2 μS/m. After drying in air at 120 °C for 12 h, the dried catalysts were calcined at 450 °C for 2 h. The calcined catalysts were pressed at 10 MPa to form pellets and the pellets were crushed to form small-sized particles with particle sizes ranging from 0.45 to 0.9 mm. The compositions of the as-prepared Cu–Zn–Ce catalysts according to those in their precursors are listed in Table 1.

2.2 Characterization

X-ray diffraction (XRD) was used to examine the bulk chemical structures of the calcined and reduced catalysts. The XRD data were recorded by a Rigaku D/Max2500 diffractometer using Cu-Kα radiation (1.5418 Å) with Ni filter, scanning from 20 to 80° (2θ). The crystallite sizes of the Cu° (111) in the reduced catalysts were calculated by using Scherrer's equation: $D = K\lambda/(B\cos\theta)$, where K was taken as 0.9, and B was the full width of the diffraction line at half of the maximum intensity.

X-ray photoelectron spectra (XPS) and X-ray induced Auger electron spectra (XAES) of the calcined and reduced catalysts were recorded on an ESCALAB 250 spectrometer (Thermal Electron Corp.) using Al-Kα radiation (1486.6 eV). The binding energies were calculated with respect to C1s peak at 284.5 eV.

The specific surface areas and the average pore sizes of the calcined catalysts were measured on a NOVA 2000e physical adsorption apparatus by BET and BJH methods, respectively.

The reduction behaviors of the calcined catalysts were investigated by temperature programmed reduction (TPR) technique using a mixed H_2/N_2 flow (5:95 v/v) of 30 mL/min and 50 mg of the calcined catalyst at a temperature ramp of 10 °C/min from 25 to 400 °C. H_2 consumption was determined by analyzing the effluent gas with a thermal conductivity detector. The calcined catalysts were preheated in air at 400 °C before the TPR measurement in order to eliminate impurities and adsorbed water.

Table 1 The compositions, specific surface areas and average pore diameters of the calcined Cu–Zn–Ce catalysts

Samples	Atomic ratios			Average pore diameters (nm)	Specific surface areas (m^2/g)
	Cu	Zn	Ce		
C1	1	2	0.5	3.8	52.4
C2	1	2	1	4.9	67.2
C3	1	2	2	3.4	67.3
C4	2	2	1	4.9	58.3
C5	2	2	2	2.7	58.7
C6	1	0	2	3.8	66.4

2.3 Catalytic Test

The catalytic test was carried out in a stainless steel tubular fixed-bed reactor with diameter and length of 8 and 200 mm, respectively, packed with 5 mL of catalyst with particle sizes ranging from 0.45 to 0.9 mm, operating at 220–280 °C and 1 MPa. The reactor was fed with a stream of MA and *n*-butanol solution (12:88 w/w) in hydrogen, the liquid space velocity was 0.2 h^{-1}, and the molar ratio of H_2 to MA was 50:1. Before catalytic test, the catalyst was firstly reduced in a mixed H_2/N_2 (10:90 v/v) stream with a flow rate of 250 mL/min from 25 to 280 °C at a temperature ramp of 1.5 °C/min. Then the catalyst was continuously reduced at 280 °C for 2 h in a mixed H_2/N_2 (30:70 v/v) stream with a flow rate of 250 mL/min. The reaction products were condensed in an ice water bath and collected at different reaction temperatures after reaction for 1 h. The collected reaction products were analyzed by a gas chromatograph, equipped with FID and a PEG packed capillary column (0.25 mm × 30 m).

3 Results and Discussion

3.1 Characterization of Catalyst

3.1.1 XRD Analysis

The XRD patterns of the calcined and reduced Cu–Zn–Ce catalysts are shown in Figs. 1 and 2. The XRD patterns of the calcined Cu–Zn–Ce catalysts exhibit the characteristic peaks of CuO (PDF#48-1548), ZnO (PDF#36-1451), and CeO_2 (PDF#43-1002), appearing at $2\theta = 35.5$, 38.7; 31.8, 34.4, 36.3, 56.6, 62.9, 68.0; 28.5, 33.1, 47.5, 56.3, 76.9°, respectively. The XRD patterns of the reduced Cu–Zn–Ce catalysts show that CuO was reduced to Cu° (PDF#04-0836) with the characteristic peaks appearing at $2\theta = 43.3$, 50.4, and 74.1° and that zinc species and cerium species were still present in the form of ZnO and CeO_2.

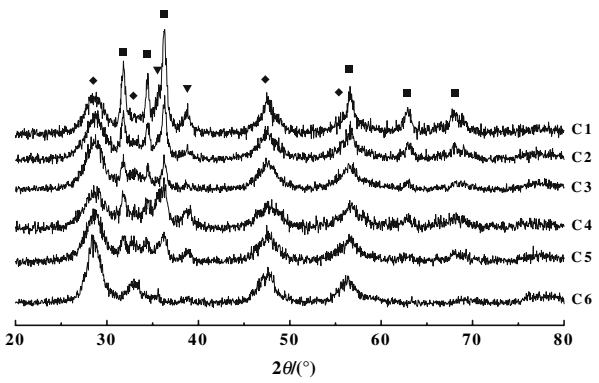

Fig. 1 XRD patterns of the calcined Cu–Zn–Ce catalysts. ▼, CuO; ■, ZnO; ◆, CeO_2

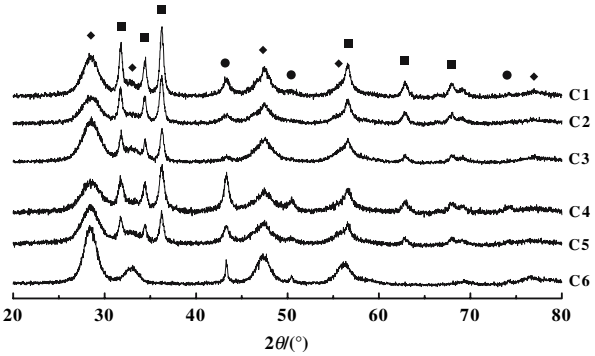

Fig. 2 XRD patterns of the reduced Cu–Zn–Ce catalysts. ●, Cu°; ■, ZnO; ◆, CeO_2

As far as the reduced catalysts are concerned, the crystallite sizes (*D*) of metallic copper (111) were estimated by Scherrer's equation. For the Cu–Zn–Ce catalysts (C1-5), the crystallite sizes of metallic copper were between 9.5 and 14.4 nm (Table 2). For the Cu–Ce catalyst (C6), the crystallite size of metallic copper was 24.6 nm. The presence of ZnO promotes the dispersivity of metallic copper.

3.1.2 XPS Analysis

The chemical states of the representative calcined Cu–Zn–Ce (C5), calcined Cu–Ce (C6), and H_2-reduced Cu–Zn–Ce (C5*) catalysts were evaluated by XPS. Figure 3a shows the $Cu2p_{3/2}$ and $Cu2p_{1/2}$ peaks of the calcined and H_2-reduced samples. The calcined samples C5 and C6 displayed the principal $Cu2p_{3/2}$ and $Cu2p_{1/2}$ peaks at 933.65, 953.45; 933.4, 953.4 eV, respectively, which is characteristic of Cu^{2+} species [18]. The binding energies of $Cu2p_{3/2}$ and $Cu2p_{1/2}$ of Cu–Ce (C6) shifted to lower values than that of Cu–Zn–Ce (C5), revealing that the chemical state of CuO is influenced by the composition of the catalyst.

After reduction, the $Cu2p_{3/2}$ and $Cu2p_{1/2}$ peaks of Cu–Zn–Ce catalyst (C5*) shifted to lower binding energies at 932.6 and 952.7 eV, respectively, meaning that after reduction, the copper species are Cu^+ or Cu°, rather than Cu^{2+} [18, 19]. The shift of $Cu2p_{3/2}$ reveals the disappearance of cupric oxide, but does not allow to reach a conclusion about the presence of solely cuprous oxide or solely metallic copper or both since the $Cu2p_{3/2}$ peaks for metallic copper and Cu_2O appear with the same binding

Table 2 The crystallite sizes of metallic copper (111) of reduced catalysts

Samples	C1	C2	C3	C4	C5	C6
D (nm)	12.0	10.5	9.5	14.4	13.6	24.6

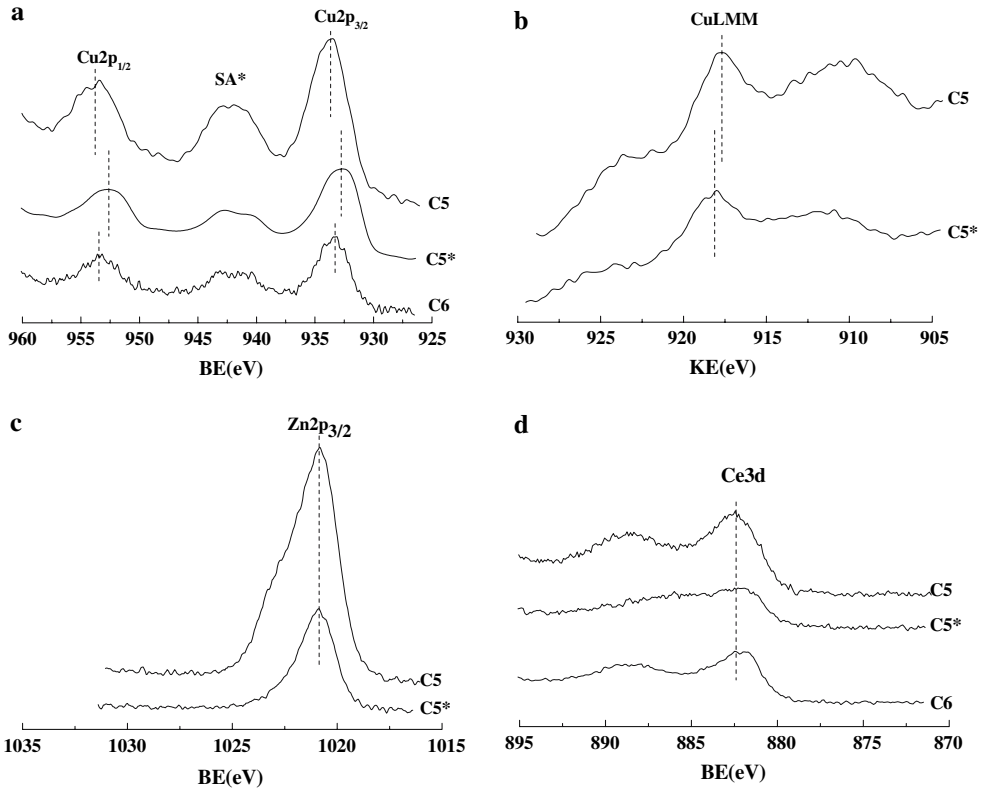

Fig. 3 X-ray photoelectron spectra of the calcined catalysts (C5 and C6) and the reduced catalyst C5 (denoted as C5*). (**a**), (**c**), and (**d**), the XPS spectra of $Cu2p_{3/2}$, $Zn2p_{3/2}$, and Ce3d of the calcined and reduced catalysts; (**b**), the XPS spectra of CuLMM of the calcined and reduced catalysts

energy. To determine the chemical state of Cu^+ or Cu°, modified Auger parameter (α') is used by many researchers [20, 21].

$$\alpha' = \mathrm{BE} + \mathrm{KE}$$

where, BE is the binding energy of the $Cu2p_{3/2}$ core level and KE is the kinetic energy of the CuLMM Auger electron. For the reduced Cu–Zn–Ce catalyst (C5*), the KE is 917.82 eV (Fig. 3b) and the α' value is 1850.42 eV. The value of the modified Auger parameter (α') is consistent with that reported by Ji et al. [21], meaning that Cu° is the main copper species in the reduced catalyst. The conclusion is also certified by the above-mentioned XRD analysis.

The $Zn2p_{3/2}$ binding energies of the calcined and reduced Cu–Zn–Ce catalysts (C5 and C5*) were 1020.85 and 1020.9 eV, respectively, pertaining to that of ZnO (Fig. 3c). The Ce3d binding energies of the calcined and reduced Cu–Zn–Ce catalysts (C5 and C5*) and the calcined Cu–Ce catalyst (C6) were 898.65, 898.7, and 898.6 eV, respectively, revealing that cerium species existed in CeO_2 (Fig. 3d).

3.1.3 TPR Analysis

The TPR curves of the calcined samples are shown in Fig. 4. For the catalysts C1–3 with a low copper content, the temperatures at the maximum reduction peaks decreased from 154 to 135 °C with increasing the CeO_2 content, indicating that the chemical state of CuO was synergistically affected by both ZnO and CeO_2, in consistent with the XPS analysis. However, for the catalysts C4 and C5 with a high copper content, the temperatures at the maximum reduction peaks were 149 and 152 °C, respectively, being almost the same as each other. After reduction, the Cu° sizes of the catalysts C4 and C5 with a high copper content were larger than that of the catalysts

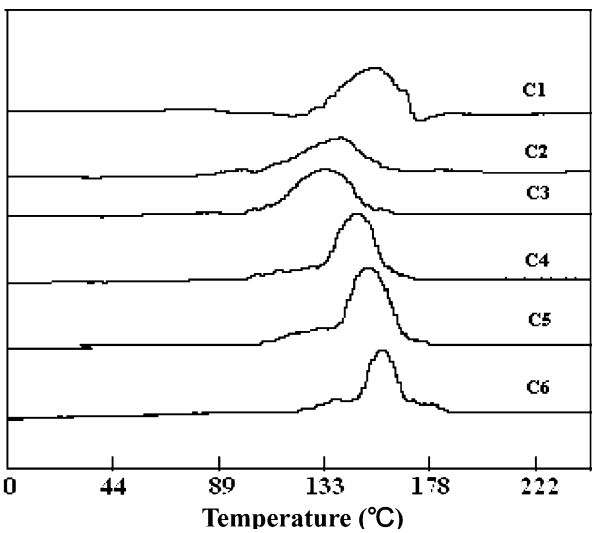

Fig. 4 TPR profiles of the Cu–Zn–Ce catalysts

C2 and C3 with a low copper content (Table 2). Therefore, it is reasonable to conclude that the formation of large-sized CuO results in a high reduction temperature.

Comparing the TPR curves of the catalysts C3 (Cu–Zn–Ce) and C6 (Cu–Ce), we found that the temperature at the maximum reduction peak of C6 (157 °C) was obviously higher than that of the catalyst C3 (135 °C). The presence of ZnO was beneficial to the dispersion of CuO, giving a low reduction temperature.

3.1.4 Specific Surface Area and Average Pore Size

The specific surface areas and the average pore sizes of the Cu–Zn–Ce catalysts are listed in Table 1. The specific surface areas are more than 52.4 m^2/g, revealing that the as-prepared catalysts have high surface areas. The range of the average pore sizes is from 2.7 to 4.9 nm, which are appropriate for hydrogenation of MA [22].

3.2 Catalytic Test

3.2.1 Hydrogenation of MA

The catalytic hydrogenation of MA by copper-based catalyst proceeds via consecutive hydrogenation steps, in which succinic anhydride, GBL, 1,4-butanediol, and THF are formed subsequently. The resultant succinic anhydride can react with the solvent, *n*-butanol, to produce dibutyl succinate (DS) [4].

Table 3 shows the catalytic activities of the Cu–Zn–Ce and Cu–Ce catalysts (C1–6) for hydrogenation of MA at 1 MPa and 220–280 °C. The experimental results show

Table 3 Catalytic activities of the Cu–Zn–Ce catalysts in maleic anhydride hydrogenation and *n*-butanol dehydrogenation[a]

Samples	*T* (°C)	*X* (MA) (%)	*S* (%)			*X*(BU) (%)	*S* (%)		H_2%
			THF	GBL	DS		BA	BB	
C1	265	98.15	5.04	66.46	28.50	9.86	20.09	79.91	47.63
	250	99.07	3.53	71.53	24.94	6.46	29.26	70.74	30.42
	235	99.07	2.73	70.93	26.34	4.55	31.03	68.97	21.78
	220	99.07	3.22	71.55	25.23	2.68	26.81	73.19	12.67
C2	280	97.22	5.04	66.04	28.92	8.17	54.08	45.92	39.96
	265	98.15	3.14	70.97	25.89	7.61	52.28	47.72	36.57
	250	98.15	4.43	70.33	25.24	5.59	58.89	41.11	26.44
	235	98.15	3.85	72.31	23.84	3.84	53.79	46.21	18.05
C3	280	98.61	2.60	73.90	23.50	7.23	41.61	58.39	34.07
	265	98.84	4.16	60.92	34.92	5.98	51.41	48.59	30.43
	250	98.38	4.00	62.07	33.93	5.28	61.24	38.76	26.80
	235	99.07	6.10	57.56	36.34	3.27	58.53	41.47	16.52
	220	99.07	4.19	54.88	40.93	1.90	57.04	42.96	10.18
C4	265	98.61	5.08	69.42	25.50	7.39	42.61	57.39	34.70
	250	98.84	3.79	70.10	26.11	5.81	55.87	44.13	27.64
	235	98.38	3.65	74.87	21.48	4.18	53.00	47.00	19.30
	220	99.07	4.52	75.32	20.16	2.73	53.36	46.64	12.29
C5	265	98.61	2.71	77.18	20.11	6.67	39.30	60.70	30.62
	250	99.07	2.65	81.47	15.88	5.52	50.10	49.90	24.46
	235	98.84	3.82	78.86	17.32	2.90	42.45	57.55	12.88
	220	99.07	3.01	73.34	23.65	1.96	60.83	39.17	9.19
C6	265	98.15	5.89	56.19	37.92	11.52	16.24	83.76	59.67
	250	99.07	3.40	87.30	9.30	7.55	14.54	85.46	31.72
	235	99.07	2.36	91.93	5.72	3.72	15.93	84.07	15.37
	220	98.15	1.57	45.89	52.55	1.70	42.82	57.18	10.51

[a] (1) MA, maleic anhydride; THF, tetrahydrofuran; GBL, γ-butyrolactone; DS, dibutyl succinate; BU, *n*-butanol; BA, butyl aldehyde; BB, butyl butyrate; *X*, conversion; *S*, selectivity. (2) The conversion of *n*-butanol (X(BU)) only concerned with the formation of butyl aldehyde and butyl butyrate. (3) $H_2\%$ = (the amount of hydrogen produced in *n*-butanol dehydrogenation/the amount of hydrogen consumed in MA hydrogenation) × 100%

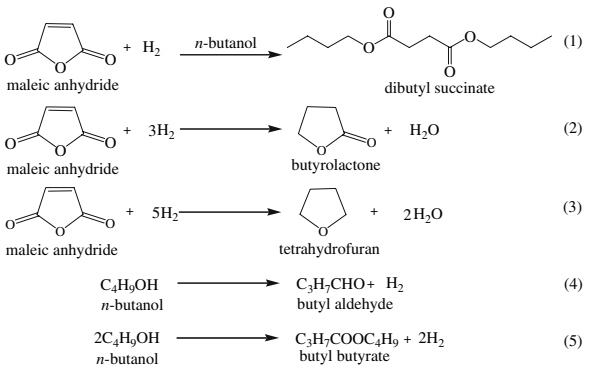

Scheme 1 Routes of hydrogen production and consumption

that the conversion of MA was more than 97%, revealing that the catalysts exhibit good activity for the hydrogenation of MA. The main product was GBL and the byproducts were THF and DS.

When the Cu–Zn–Ce catalysts, C1 and C2, with a low copper content were used, the selectivities of GBL, THF, and DS were in the ranges of 66.04–72.31%, 2.73–5.04%, and 23.84–28.92%, respectively at the reaction temperatures ranging from 220 to 280 °C. The selectivities were not significantly affected by the reaction temperature, meaning that the catalysts C1 and C2 with low copper and cerium contents exhibited good catalytic activity. However, when the cerium content was further elevated (C3), the selectivity of GBL rapidly decreased from 73.90 to 54.88%, while the selectivity of DS rapidly increased from 23.5 to 40.93%, with decreasing the reaction temperatures from 280 to 220 °C. Therefore, for the catalysts with a low copper content, the exceeding CeO_2 deteriorated the catalytic activity of the Cu–Zn–Ce catalyst.

For the catalysts, C4 and C5, with a high copper content, the selectivities of GBL, THF, and DS were 69.42–75.32%, 3.65–5.08%, 20.16–26.11%; 73.34–81.47%, 2.65–3.82%, 15.88–23.65%, respectively, at the reaction temperatures ranging from 220 to 265 °C. As compared the catalytic activities of the catalysts C4 and C5, it was found that the catalytic activity of the catalyst with a high copper content was enhanced by increasing the CeO_2 content and not significantly affected by the reaction temperature. Moreover, the activities of the catalysts with a high copper content (C4 and C5) were higher than that with a low copper content (C1–3).

For the Cu–Ce catalyst (C6) without ZnO, the selectivities of GBL, THF, and DS ranged from 45.89 to 91.93%, 1.57 to 5.89%, and 5.72 to 52.55%, respectively. A maximum GBL selectivity of 91.93% appeared at 235 °C in the reaction temperature range of 220–265 °C. The catalytic activity of the Cu–Ce catalyst was significantly affected by the reaction temperature.

3.2.2 *Dehydrogenation of* n-*Butanol*

Copper-based catalyst is used not only for hydrogenation but also for dehydrogenation. In the dehydrogenation process, *n*-butanol is firstly dehydrogenated to form butyl aldehyde; the resultant butyl aldehyde is converted to butyric acid and *n*-butanol via a disproportionation reaction; then the resultant butyric acid and *n*-butanol is converted to butyl butyrate via an esterification reaction [4, 14]. The catalytic activities of the Cu–Zn–Ce catalysts in the dehydrogenation of *n*-butanol to butyl aldehyde and butyl butyrate are also listed in Table 3. For the Cu–Zn–Ce catalysts C1–5, the conversion of *n*-butanol, in a range of 1.9–9.86%, increased with elevating the reaction temperature. The selectivities of butyl butyrate and butyl aldehyde were in the ranges of 39.17–79.91% and 20.09–60.83%, respectively. In general, the selectivity of butyl butyrate increased, while the selectivity of butyl aldehyde decreased, with the increasing of the reaction temperature. For the Cu–Ce catalyst, a maximum *n*-butanol conversion of 11.52% appeared at 265 °C and the selectivity of butyl butyrate was more than 83% in the reaction temperature range of 235–265 °C. By comparing the activities of Cu–Zn–Ce and Cu–Ce catalysts in *n*-butanol dehydrogenation, it can be concluded that the activity of Cu–Ce catalyst is higher than that of Cu–Zn–Ce catalysts. It is worth noting that butyric acid as an intermediate product was not detected in the dehydrogenation process. This result reveals that the esterification between the resultant butyric acid and *n*-butanol is quite rapid.

3.2.3 *Compensation Between the Hydrogenation and the Dehydrogenation*

Hydrogen produced by the *n*-butanol dehydrogenation can be used as a feedstock for the MA hydrogenation. The ratios of the hydrogen produced in *n*-butanol dehydrogenation to the hydrogen consumed in MA hydrogenation (H_2%) were calculated according to Scheme 1 and listed in Table 3.

In the coupling process of hydrogenation and dehydrogenation catalyzed by Cu–Zn–Ce catalysts (C1–5), the H_2% values, in a range of 9.19–47.63%, increased with elevating reaction temperature from 220 to 280 °C. On the other hand, the H_2% values of the Cu–Ce catalyst (C6) increased from 10.51 to 59.67% with elevating the reaction temperature from 220 to 265 °C. Therefore, Cu–Zn–Ce and Cu–Ce catalysts are beneficial to the H_2 compensation in the coupling process.

4 Conclusions

The XRD and XPS analyses both proved that Cu° is the active component in the reduced Cu–Zn–Ce and Cu–Ce

catalysts. The presence of ZnO promotes the reduction of copper oxide to metallic copper and enhances the dispersion of Cu° in catalyst. The catalytic activity of Cu–Zn–Ce catalyst in MA hydrogenation to GBL is synergistically affected by CeO_2 and ZnO.

The catalytic activity of Cu–Zn–Ce catalyst in the hydrogenation of MA to GBL is not significantly affected by the reaction temperature. On the other hand, in the absence of ZnO, the catalytic activity of Cu–Ce catalyst is significantly affected by the reaction temperature.

The Cu–Zn–Ce and Cu–Ce catalysts exhibit well catalytic performance not only for hydrogenation but also for dehydrogenation. The ratios of the hydrogen produced in *n*-butanol dehydrogenation to the hydrogen consumed in MA hydrogenation (H_2%) increase with elevating the reaction temperature.

Acknowledgments The work was financially supported by Jiangsu Province, China (200470) and Zhenjiang Science and Technology Bureau (CZ2006006). Authors sincerely thank Professor Jianxin Wu at University of Science and Technology, China, for XPS measurement and Professor Kangmin Chen at Jiangsu University for XRD measurement.

References

1. Hara Y, Takahashib K (2002) Catal Surveys from Jpn 6:73
2. Jung SM, Godard E, Jung SY, Park K-C, Choi JU (2003) J Mol Catal A: Chem 198:297
3. Brownstein AM (1991) Chem Tech 21:506
4. Hu T, Yin H, Zhang R, Wu H, Jiang T, Wada YJ (2007) Catal Commun 8:193
5. Herrmann U, Emig G (1998) Ind Eng Chem Res 37:759
6. Herrmann U, Emig G (1997) Ind Eng Chem Res 36:2885
7. Castiglioni GL, Vaccari A, Fierro G, Inversi M, Lo Jacono M, Minelli G, Pettiti I, Porta P, Gazzano M (1995) Appl Catal A Gen 123:123
8. Castiglioni GL, Ferrari M, Guercio A, Vaccari A, Lancia R, Fumagalli C (1996) Catal Today 27:181
9. Liu Z, Liao J Tan J, L D (2001) Indus Catal 6:41
10. Aneggi E, Boaro M, Leitenburg C, Dolcetti G, Trovarelli A (2006) J Alloys Compd 408:1096
11. Zhu YL, Yang J, Dong GQ, Zheng HY, Zhang HH, Xiang HW, Li YW (2005) Appl Catal B: Environ 57:183
12. Abashar MEE (2004) Chem Eng Process 43:1195
13. Yang J, Zheng HY, Zhu YL, Zhao GW, Zhang CH, Teng BT, Xiang HW, Li Y (2004) Catal Commun 5:505
14. Elliott DJ, Pennella F (1989) J Catal 119:359
15. Wang HJ, Duan QW (2003) Speciality Petrochem (Chinese) 1:20
16. Müller SP, Kucher M, Ohlinger C, Kraushaar-Czarnetzkyi B (2003) J Catal 218:419
17. Girol SG, Strunskus T, Muhler M, Wöll C (2004) J Phys Chem B 108:13736
18. Figueiredo RT, Martinez-Arias A, Granados ML, Fierro LG (1998) J Catal 178:146
19. Mankowski G, Duthil JP, Giusti A (1997) Corros Sci 39:27
20. Velu S, Suzuki K, Gopinath CS, Yoshida H, Hattori T (2002) Phys Chem Chem Phys 4:1990
21. Ji D, Zhu W, Wang Z, Wang G (2007) Catal Commun 8:1891
22. Li J, Jiang Y, Cheng JY, Wang HM (2000) Chin J Appl Chem 17:379